

Analysis of tomographic mineralogical data using YaDiV—Overview and practical case study

Karl-Ingo Friese^{a,*}, Sarah B. Cichy^b, Franz-Erich Wolter^a, Roman E. Botcharnikov^b

^a *Welfenlab, Institut fuer Mensch-Maschine-Kommunikation, Leibniz Universität Hannover, Welfengarten 1, 30167 Hannover, Germany*

^b *Institut für Mineralogie, Leibniz Universität Hannover, Callinstr. 3, 30167 Hannover, Germany*

ARTICLE INFO

Article history:

Received 22 August 2012

Received in revised form

16 January 2013

Accepted 31 January 2013

Available online 16 February 2013

Keywords:

3D

Segmentation

Visualization

Geology

Rock texture

ABSTRACT

We introduce the 3D-segmentation and -visualization software YaDiV to the mineralogical application of rock texture analysis. YaDiV has been originally designed to process medical DICOM datasets. But due to software advancements and additional plugins, this open-source software can now be easily used for the fast quantitative morphological characterization of geological objects from tomographic datasets.

In this paper, we give a summary of YaDiV's features and demonstrate the advantages of 3D-stereographic visualization and the accuracy of 3D-segmentation for the analysis of geological samples. For this purpose, we present a virtual and a real use case (here: experimentally crystallized and vesiculated magmatic rocks, corresponding to the composition of the 1991–1995 Unzen eruption, Japan). Especially the spacial representation of structures in YaDiV allows an immediate, intuitive understanding of the 3D-structures, which may not become clear by only looking on 2D-images. We compare our results of object number density calculations with the established classical stereological 3D-correction methods for 2D-images and show that it was possible to achieve a seriously higher quality and accuracy.

The methods described in this paper are not dependent on the nature of the object. The fact, that YaDiV is open-source and users with programming skills can create new plugins themselves, may allow this platform to become applicable to a variety of geological scenarios from the analysis of textures in tiny rock samples to the interpretation of global geophysical data, as long as the data are provided in tomographic form.

© 2013 Elsevier Ltd. All rights reserved.

1. Introduction

3D-image analysis techniques become popular in diverse fields of research. Starting with medicine, where 3D-methods are already commonly used, mechanical engineering and geology (see e.g., [Ketcham, 2005](#)) also started to exploit the new possibilities. Especially petrologists are interested in textural analysis provided by μ -tomography of vesicles and crystals in rocks (see review by [Baker et al., 2012](#)).

The quantitative description of object morphology can provide important insights into the geological evolution of rocks. A variety of analytical methods have been developed to record 3D-rock textures either by two-dimensional photographs, taken with conventional or microscopy cameras, or by three-dimensional

tomography in geophysics and microanalysis. The main disadvantage of the 2D-image analysis is the requirement for 3D-correction, whereas tomographic scandata (or serial sectioning) allows direct 3D-analysis. Although up to this date, there are limitations concerning X-ray μ -tomographic imaging of mineralogical samples. Especially the separation of individual objects of interest in highly vesiculated or crystallized samples is not clear in tomographic projection images based only on density differences (see review by [Baker et al., 2012](#)). The quantitative interpretation of morphological characteristics can be achieved by applying computer software programs. Commonly used 3D-computer programs in this field (*MATLAB*, *AVIZO*, etc.) usually need high-capacity hardware (internal storage, graphic cards, etc.), have restricted tool properties and are expensive in licensing. Here, we want to present our own open-source 3D-segmentation and -visualization software (*YaDiV*¹) that allows the interactive visualization of large datasets, while requiring relatively low hardware capacity. We will give an example of real

* Corresponding author. Tel.: +49 511 762 2913; fax: +49 511 762 2911.

E-mail addresses: kif@gdv.uni-hannover.de, kif@welfenlab.de (K.-I. Friese), s.cichy@mineralogie.uni-hannover.de (S.B. Cichy), few@gdv.uni-hannover.de (F.-E. Wolter), r.botcharnikov@mineralogie.uni-hannover.de (R.E. Botcharnikov).

¹ <http://www.welfenlab.de/en/yadiv>, see also [Friese et al. \(2011\)](#).

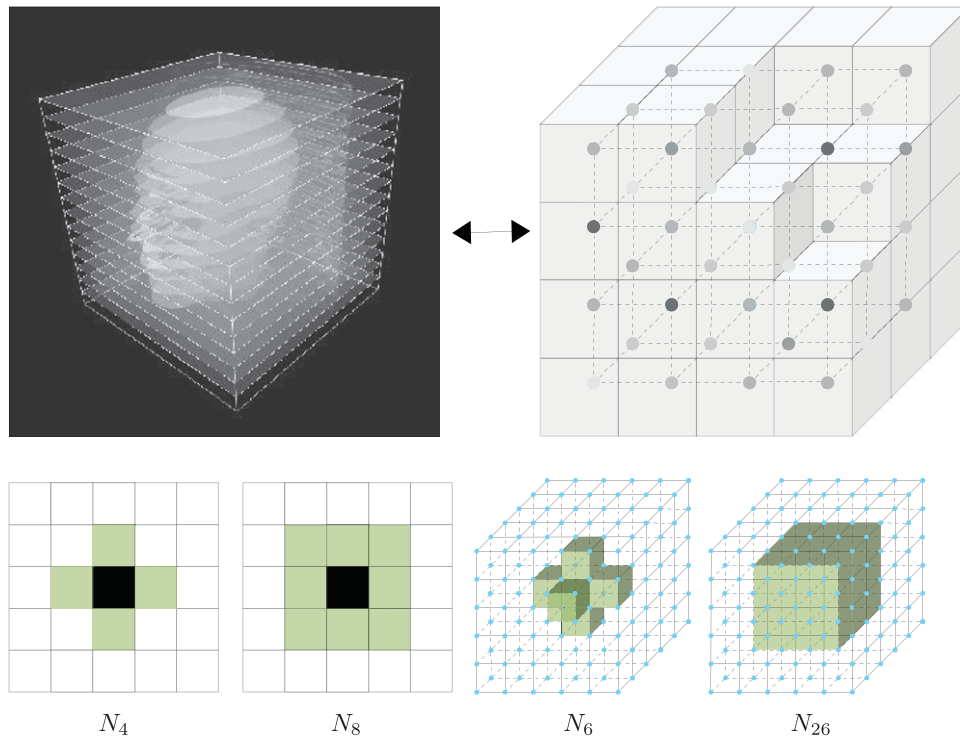


Fig. 1. Tomography data seen as a regular grid.

rock texture analysis and (to our knowledge) an one of a kind investigation on the accuracy of tomographic textural analysis (using YaDiV) in comparison to conventional stereological 3D-correction methods of 2D-image derived parameters of a virtual sample.

2. 3D-image analysis

For several years, 3D-imaging methods have been used in modern medicine for a wide range of applications. Tomographic (Greek: *tomos*="part" and *graphein*="to write") data can be obtained by different imaging methods, e.g., computed tomography (CT), magnetic resonance tomography (MRT) or positron emission tomography (PET). These methods use a single physical effect to obtain a set of 2D-images (slices) of a certain part of the scanned object. Often these images are taken in equidistant intervals orthogonal along one axis. Mathematically, the generated data structure is called a *regular grid* (see Serra, 1982).

Hence, a (3D-)regular grid can be understood as a discrete set of values in \mathbb{R}^3 distributed with constant spacing along each axis (spacing can differ between any two axes). The cells, formed by eight adjacent grid points, are shaped like bricks, illustrated in Fig. 1. Common examples of 2D-regular grids are classic images, here the grid points are called pixels (picture elements). In the 3D-case, grid points are called voxels (volumetric elements). Please note, that in this context, a voxel is not a cube and likewise a pixel no little square—even if this is sometimes used in figures for easier understanding. Instead, both are understood as values at discrete positions in the regular grid (see Smith, 1995 for a more detailed discussion).

In the following, we always consider a grid to be regular. Adjacent grid points are called neighbors. If only orthogonal adjacent grid points are considered, we will speak of a N_4 neighborhood in 2D and N_6 in 3D. If also diagonally adjacent pixels/voxels are allowed, the neighborhood will be called N_8 in 2D and N_{26} in 3D (named by the number of neighbors, see Fig. 1).

3D-imaging methods measure different effects than the natural reflection of light, therefore a *transfer function* has to be defined mapping the measured values, e.g., density or heat, into color values, often combined with transparency. If the grid also contains structural meta-information (see Section 2.3) given by the user, this meta-information can also be used in the visualization.

2.1. Slice image vs. volume visualization

A simple way to visualize and analyze tomographic data is to look at individual 2D-slices. While this is a good first approach which can be done with tools like Adobe Photoshop, GIMP² or ImageJ,³ it is not suited for a solid analysis of 3D-structures. A classic example are conic sections, where a cone – a very simple geometric object – is intersected with a 2D-plane. The resulting image can show a parabola, a circle, an ellipse, one or two straight lines or a single point. Looking only at this slice image, the nature of the original can only be guessed.

Natural and more complex structures lead to an even wider range of cut-forms which is often the cause of false conclusions. Distances and angles measured in 2D are not only depend on the z-position of the slice image but also on the object alignment inside the grid. Fig. 2 shows a porous geological sample scanned in 2D (left) and 3D (right). The 2D-image suggests that it consists of two materials visualized by two different color values (light gray dark gray) and it appears that the darker material represents a number of individual pores inside the lighter matrix. But the 3D-visualization illustrates, that large parts of the dark material are connected in a complex manner representing a single object (pore) with a complex 3D-morphology, invisible in the 2D-slide. The connected pores have been segmented in Fig. 2b, as indicated by the different colors in the picture. The exact 3D-shape of this

² <http://www.gimp.org>.

³ <http://rsb.info.nih.gov/ij/>.

porous sample can be best understood with an interactive, moving 3D-stereo visualization (similar to 3D-movies like “Avatar”).

2.2. 3D-visualization

The first and natural approach to analyze 3D-volume data is to simply look at it. This very intuitive form of data exploration can give quick insights and deeper understanding, e.g., by noticing that objects inside a geological sample are aligned along a common axis.

Classic 3D-visualization renders a single 2D-image on a standard monitor—comparable to a perspectively drawn image. Both can be convincing, as the human brain generates a 3D-illusion, taking into account shading and object size information. However, a natural, intuitive and realistic impression can only be achieved with VR-hardware, generating two perspective pictures, one for each eye. This technique is called *stereoscopic visualization*.

Volume visualization methods are usually separated into *direct* and *indirect* approaches. Direct methods (e.g., ray casting in Kajiya and Herzen, 1984 or splatting in Westover, 1991) directly create a viewable image from the 3D-grid data. Indirect methods (marching cubes in Lorenzen and Cline, 1987, marching tetrahedron in Carneiro et al., 1996,...) first extract a boundary surface, which can then be visualized using standard 3D-graphic hardware. This results in a very fast visualization, where objects can be explored in real time by walking/flying around them.

2.3. 3D-segmentation

Segmentation describes the process of localizing structures of interest in the grid data, e.g., a specific human organ (in a medical context) or a texture in geological samples. Technically spoken, a *segment* is a selection of grid points of the original data, that is in

some sense meaningful for a human user. The most basic way to define such a segment would be manual selection of individual grid points, with an interface similar to a common painting program. This often used technique can become very time expensive.

To overcome this, there exists a number of (semi-)automatic segmentation methods, which are usually classified by their underlying concepts (edge detection, histogram based, level-set based, etc.). A different approach is to classify them by their application, resulting in

- *general methods* that can be used on a priori structures or
- *model-based methods* which are designed for a special case. They can exploit model-specific information like density, texture or form parameters (topology, curvature,...).

An example for a simple general method is to select voxels within an intensity *range* defined by a given minimum and maximum. Another supportive general method is (seeded) *region growing*. A given (user-selected) starting point is used to expand the segmented area by extending it to the neighborhood as long as a similarity criterion is fulfilled, e.g., a small difference in the voxel value (see Fig. 3). Different techniques can be used to enhance the basic concept, e.g., by defining blocking regions or allowing multiple seeds. Other methods, such as *edge detection* can be used to detect edges in the volume to define segment contours.

All general methods have in common that for real world data, usually not a single one of them will give the desired result but several of them have to be combined. This can be achieved by using volumetric boolean operations that allow to add or subtract two segments.

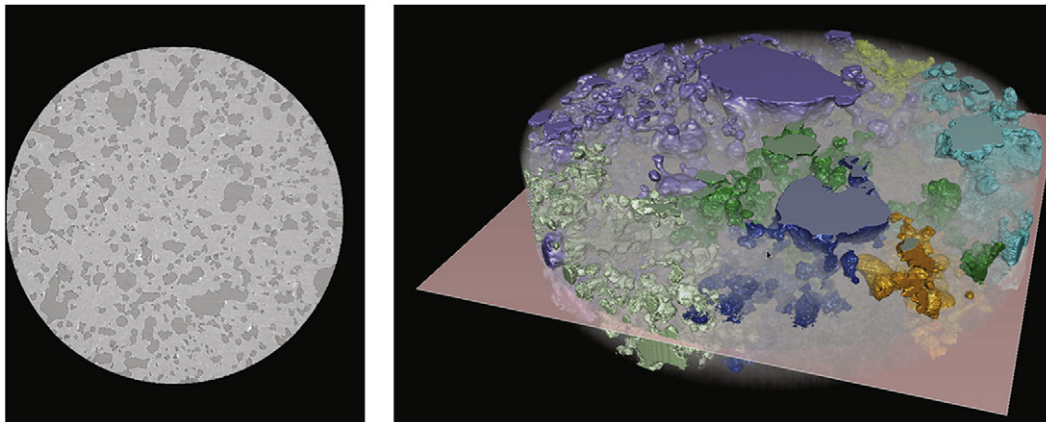


Fig. 2. 2D- and 3D-visualization of tomography data in YaDiV.

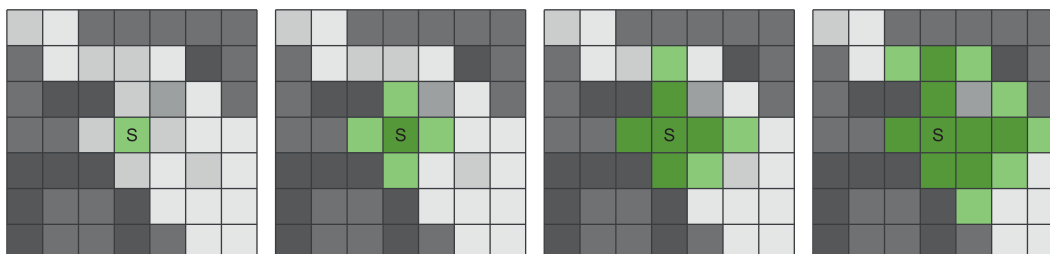


Fig. 3. Expansion of region grow method (2D, N_4).

Model-based methods usually produce the best results, but are expensive to develop. They need to be adapted to every new case and cannot be used for scans which are either unknown or differ strongly from the standard situation. One important class of model-based methods is deformable model approaches (see Cohen, 1991 or McInerney and Terzopoulos, 1996). An initial shape is placed inside the to-be-segmented structure and treated as if it would be a balloon filled with air. During the segmentation process, the initial shape expands (in normal direction) and is slowed by a shape-preserving force and by image forces (e.g., high gradient). The initial shape and expansion parameters can be modified to adapt the deformable model approach to new situations.

3. YaDiV

YaDiV is an open-source software for 3D-visualization and -segmentation of volume data, developed by Karl-Ingo Friese at the Welfenlab in Hannover, Germany. Here we only present a summary of YaDiV's features; details of its models, algorithms and structures can be obtained from former publications (see Friese, 2010; Friese et al., 2011). Being implemented in Java, YaDiV is platform-independent and can even be run from USB-stick without installation. Unlike other programs in this area (e.g., 3D-Slicer or Osirix) it is not ITK/VTK-based and was developed from scratch.

YaDiV supports multi-threading for time-consuming methods, taking advantage of modern multi-core architectures. A side effect is that the graphical user interface (GUI) is never blocked: All processes can be observed with an animated visualization of the intermediate results and manually aborted at every stage. The software is designed to become an open platform for the rapid development of new modules. It contains a large set of standard operations and a plugin interface for more specific modules.

3.1. Supported data

Originally designed for DICOM data,⁴ we extended YaDiV with an import function for standard image formats (PNG, TIFF, JPG,...), allowing to import and analyze a wide range of tomographic data. When importing standard images, it is necessary to define the spacing (in x -, y - and z -directions) as this is not stored in the image data. The import filter also includes an optional circular crop with a user-defined radius, since many imaging methods only guarantee valid measuring in a cylindrical scan area.

Additionally, it was necessary to add support for very large datasets, since scans of geological materials can become very large (up to 2048^3 voxel). This was achieved by reorganizing the central data structure to support more efficient storage mechanisms. Still, the supported maximum volume dimension strongly depends on the computer's main memory (minimum 4 GB).

3.2. Visualization

YaDiV supports several modules for data visualization. Beside classic 2D-visualization, it is possible to explore the data in 3D, including support for stereo displays. The fast and interactive visualization methods allow an intuitive, experimental data exploration even by inexperienced users and often lead to new insights and understanding.

The volume visualization techniques include two fast and interactive texture-based approaches and a ray casting module. While *3D-texturing* produces the better visual impression, it is usually slower (depending on the graphic card) and more memory-consuming than *2D-texturing*. Both methods are fast enough to interactively explore the volume, even with stereographic devices (Fig. 4).

YaDiV also supports high-quality *ray casting* visualization. While this usually takes much longer, the image quality can be greatly enhanced. Besides normal (realistic) lighting models, artistic or illustrative rendering methods can be chosen. The ray casting module also supports the recording of high-resolution animations.

The *transfer function editor* allows to interactively explore the obtained data in 3D by setting color and transparency for different data values—the function is interpolated linearly between these user-defined control points. As an additional feature, it is possible to define spherical textures for lit-sphere mapping (see Sloan et al., 2001; Bruckner and Gröller, 2007), which belongs to the class of non-photorealistic rendering algorithms. The transfer function affects the texturing methods and ray casting module.

Segments can be visualized by their surface with a modified self-refining marching cube technique, producing continuous “watertight” triangle meshes (Fig. 4b). The segment information can also be included in the texture views, visualized as a point cloud or taken into account during ray casting.

3.3. Segmentation

Normally, a user first creates a segment, uses post-processing filters (e.g., to eliminate noise or close small holes) and finally analyzes the segment by calculating its volume and shape parameters, or exports it into various formats.

3.3.1. Creating a segment

YaDiV supports a range of general segmentation tools. More specific modules (so-called model-based algorithms, see Section 2.3) can be loaded as plugins. The general methods include:

- *Range based* segmentation, defining a segment by a lower/upper intensity threshold. This method is very fast, even for huge volume data.
- *Region grow* approach, expanding the segment area from one or more seed points as long as a given variance from the start value(s) is maintained. Supports blocking segments.
- *Edge detection* methods, using different edge detection techniques to detect edges in the volume that can be used as segment contours. This method is also very fast.
- *Level set* algorithms, evolving the segment contour based on the level set method (see Kass et al., 1988; Malladi et al., 1995), supporting an edge stopping and an energy minimization method. Both methods are mathematically challenging and are quite slow compared to range, region grow and edge detection.
- *Atlas based* segmentation, using a previously segmented volume to find similar structures in a new scan (see Rohlfing et al., 2005 for a good overview). Supports rigid and elastic registration. Again the result is visualized during the process. The segmentation time depends on the volume size and can differ from several seconds to several minutes on a normal PC.

All methods support multi-threading and visualize intermediate results animated during the process, allowing the user to

⁴ Digital Imaging and Communications in Medicine is a standard for exchanging information in medical imaging.

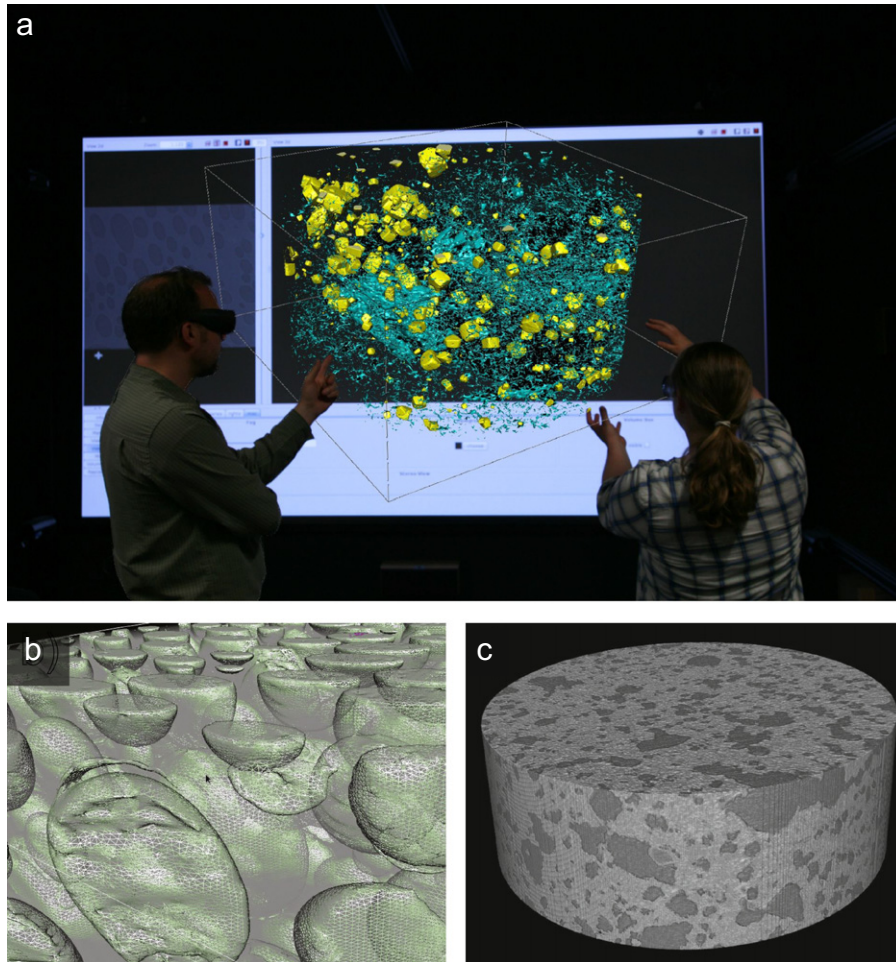


Fig. 4. (a) Interactive stereographic visualization (illustrative picture), (b) segments as triangle meshes and (c) volume visualization with YaDiV using ray casting.

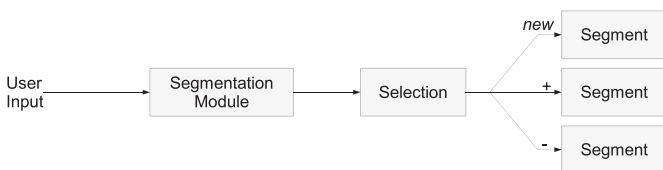


Fig. 5. Segmentation concept.

abort them at any time. It is also possible to add or remove voxels manually from a segment with an interface similar to a 2D-painting program, with different brushes and optional variance.

All segmentation methods do not directly create a new segment but modify the so-called selection. This selection can then be turned into a segment or added to/subtracted from an existing one, illustrated in Fig. 5. Also, it is possible to copy an existing segment back into the selection, allowing later post-processing.

3.3.2. Post-processing

In theory, segmentation of a well-defined structure is a straightforward and deterministic process. But real data also contains noise and imaging artifacts. Thus, YaDiV comes with a set of tools that allows selection processing, e.g., a *closing* or an *opening* operation.

By performing a dilatation–erosion pattern (grow and shrink) it is possible to close small holes in a segment (closing). Dilatation (or growing) means that all unset segment grid points adjacent to

the segment (N_8 or N_{26}) become set; the segment grows one grid point in each direction. The opposite operation, erosion (or shrink), removes all segment grid points that have an unset N_8 or N_{26} neighbor. Performing both steps will not result in the same configuration as before, since the dilatation may “fill” small holes whose grid points afterwards do not belong to the segment border anymore, illustrated in Fig. 6. The opposite (erosion–dilatation) is called opening and can e.g., be used to eliminate isolated voxels.

The *connectivity tools* (Fig. 7) allow to analyze the connected sub-structures of a segment and also supports to remove them, either manually or by a given criteria (e.g. remove all connected sub-structures with border contact or below/above a given size). Similar to the dilatation–erosion pattern, this can be used to remove noise (connected parts with very small volume) or close holes by inverting the segment, removing small parts and inverting the data again.

3.3.3. Analysis and export

Once a segment has been created, it is possible to calculate its volume and analyze its shape (e.g. the number of path-connected components using the connectivity tools). The volume calculation is done by multiplying the number of segment voxels by the volume of a voxel defined by the grid spacing. Further exported values are the minimum, maximum and mean intensity value of the connected parts and if they touch the border of the measured volume data.

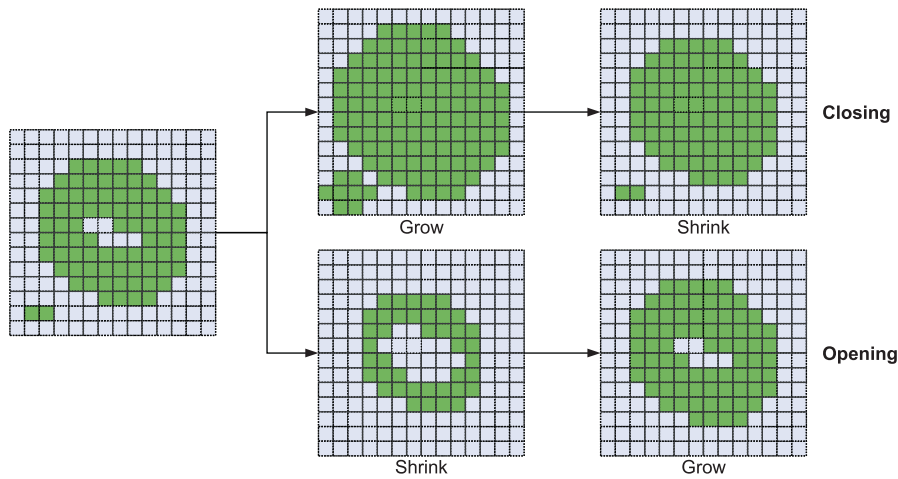


Fig. 6. Morphological operations: opening and closing.

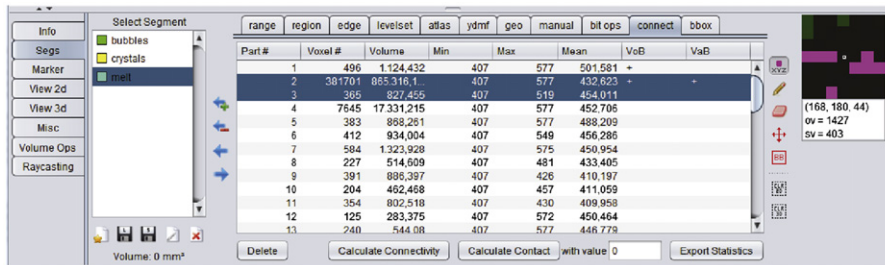


Fig. 7. Connectivity analysis and post-processing.

For further processing or analysis, a segment can be exported to different formats, e.g. the triangulated segment surface as STL⁵ mesh (binary or ASCII). The discrete grid can also be exported, e.g. as a stack of images in different formats (PNG, TIFF,...) or a set of DICOM files.

4. Geological case study—an example

A typical mineralogical task is the interpretation of rock textures, classically using 2D-images of thin-sections and applying 3D-correction methods (see Higgins, 2000, 2002, 2006a,b). With new imaging techniques it became possible to obtain true 3D-volumes from tomographic (3D-)images, which can be visualized, segmented and analyzed e.g. using YaDiV.

4.1. Origin of samples

The mineralogical samples used in this study represent experimentally decompressed and quenched synthetic rhyodacitic groundmass, which consists of silicate glass, microlites and bubbles (Cichy et al., 2010; Cichy, 2011; Nowak et al., 2011). Their textures reflect characteristic degassing and microlite crystallization processes (i.e. nucleation and growth), providing important constraints on the geologic evolution of the volcanic rocks, e.g., magma storage conditions and ascent/eruption dynamics.

4.2. Synchrotron-based X-ray μ -tomography

Our samples were analyzed at the synchrotron light source (SLS) of the Paul-Scherrer-Institute in Villigen, Switzerland. The TOMCAT (TOMographic Microscopy and Coherent rAdiology experimenTs) beamline receives photons from a 2.9 T superbending magnet with a critical energy of 11.1 keV, producing a monochromatic beam. A sample is fixed on a centering and rotation stage in front of a microscope, detecting the monochromatic X-ray beam.

This non-destructive synchrotron-based X-ray μ -tomography recorded a series of 2048 digitalized, high-resolution 2D-projection images with 256 gray levels, which depend on the chemical composition and density of the material. A typical 2D-image has a resolution of 2048 \times 2048 pixel with a pixel size of 0.74 μ m at 10 \times magnification or of 0.37 μ m at 20 \times magnification. The distance between two neighboring images and the projection depth are defined by only one pixel. Due to noise infiltration by physical properties of this analytical method, a Parzen filter was used to reconstruct and smooth the images.

4.3. Bubble number densities

Bubbles number density (BND) refers to the total number of objects per unit volume. The BND is calculated using the following equation from Gardner et al. (1999):

$$BND = \frac{\phi_m}{\sum \frac{n_i}{N_T} V_i} \quad (1)$$

where n_i and V_i are the number and volume of bubbles of a diameter i , respectively. N_T is the total number of bubbles

⁵ See <http://www.ennex.com/fabbers/StL.asp>.

measured and ϕ_m is the bubble volume fraction in the sample. For simplification, the term $n_i \cdot V_i / N_T$ can be determined for each individual object, i.e. $n_i = 1$. Classically, individual bubble areas are obtained from thin-section images using 2D-image processing and analysis softwares, e.g. ImageJ. A subsequent conversion into 3D-volumes is therefore vital. Hence, the bubble shape is either seen as an ideal ellipsoid, using the ImageJ-derived major axis of the best-fitting surrounding ellipsoid as the a -axis and the minor axis as the b - and c -axes, or we can apply the CSDcorrection⁶ software, following the method after Noguchi et al. (2008). With 3D-tomographic data it becomes possible to perform true 3D-texture analysis, reducing the unavoidable correction error of 2D-methods.

BNDs are mainly dependent on smaller-sized objects. Their absence or abundance will either decrease or increase the number densities, respectively. Although former 2D-textural studies have tried to minimize truncation effects by analyzing several images per sample at different positions and magnifications, e.g. Armienti (2008), the conversion to 3D-textures still exhibits a relatively large error. This error may be derived from the generalization of aspect ratios and circularities of the investigated objects, and from the possible effect of object coalescence which is not totally resolved by 2D-images. Poor thin-section preparation can also negatively affect the quality of the samples and its images. For example, some voids in samples can be filled with epoxy resin and abrasive materials during sample preparation, necessitating manual image editing (e.g. Cichy et al., 2010; Cichy, 2011; Nowak et al., 2011), or the rims of voids can be cracked and damaged, leading to false size determinations. Therefore, a new trend in geological investigations of rocks is the non-destructive acquisition of tomographic scans, see Ketcham (2005), Polacci et al. (2009), Baker et al. (2012). From this data, volumes and shapes can be computed with high precision, improving the BND determination and leading to negligible analytical errors.

4.4. Textural analysis

The textural analysis of the geological products described above was performed using YaDiV and also generally accepted methods of Noguchi et al. (2008) applying Higgins' CSDcorrections software (Higgins, 2000, 2002, 2006a,b). BND results for both methods are plotted in Fig. 8, showing that BNDs determined with YaDiV (diamonds) are about two log units lower than for the conventional method (circles) using only 2D-images as a source, implying that less individual bubbles per unit volume were detected by the 3D-segmentation method.

It appears to be logical that the values generated using the tomographic volume information should be more accurate. However, it is not possible to measure the exactness of both methods in natural data, as the real (exact) bubble volumes are unknown.

5. Evaluation of 2D- and 3D-image analysis

A classical problem in the evaluation of segmentation methods and image analysis is the lack of knowledge of the exact structure information. A standard way to overcome this is to have a group of experts doing the segmentation manually and compare their results with the (semi-)automated methods. Since this is not suitable for very large volume of geological data, we decided to evaluate our method by creating a virtual test scan with volumetric objects of known volumes.

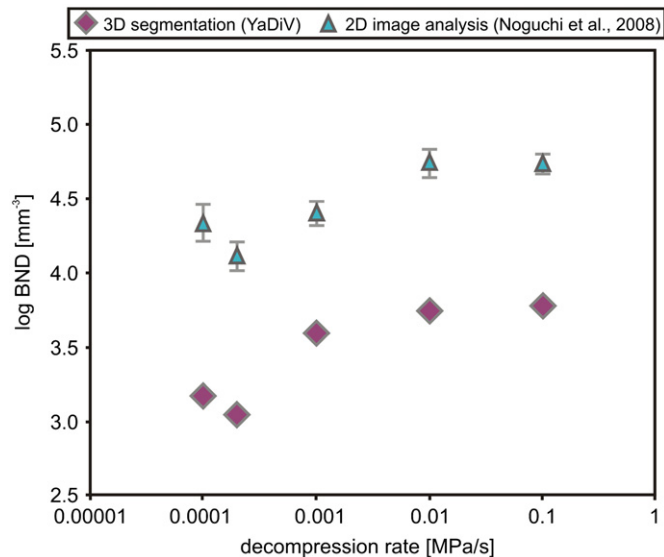


Fig. 8. Comparison of 2D- and 3D-derived bubble number densities (BND) of low-pressure decompression experiments (50–0.1 MPa, 850 °C) as a function of the decompression rate. Error bars show standard deviation (2σ) of replicate 2D-analyses. Errors for 3D-analyses are negligible.

5.1. Creating a virtual test scan

To evaluate volume calculation, connectivity measurements and bubble number densities, we implemented a YaDiV-plugin that allows us to create a virtual volume filled with randomly sized and rotated (simple) disjoint shapes where the exact number, volume and connectivity is known. The mathematical exact objects are then sampled discretely, generating a 3D-regular grid.

We used two kinds of shapes: ellipsoids and (half-)tori. Both are simple mathematical objects with well-known surface and volume. The half-tori were chosen to test shapes that have more than one connected component in the intersection with a 2D-(slice) plane. Since the calculation of the exact volume is critical for the evaluation, we will describe the creation process in detail.

5.1.1. Ellipsoids

The shape of an ellipsoid is defined by its equatorial radii a , b and c (see Fig. 9). An arbitrarily oriented, filled ellipsoid centered at v can be defined by

$$(x-v)^T A^{-1} (x-v) \leq 1 \quad (2)$$

with $x, v \in \mathbb{R}^3$ and a symmetric positive definite matrix $A \in \mathbb{R}^{3 \times 3}$. The eigenvectors of A define the principal directions of the ellipsoid, the square roots of the eigenvalues define the ellipsoid's equatorial radii. Using this knowledge, an arbitrarily oriented ellipsoid centered at $v \in \mathbb{R}^3$ with the radii $a, b, c \in \mathbb{R}_{>0}$ can be defined by a rotation matrix $M_R \in \mathbb{R}^{3 \times 3}$ and a scaling matrix

$$M_S = \begin{pmatrix} a^2 & 0 & 0 \\ 0 & b^2 & 0 \\ 0 & 0 & c^2 \end{pmatrix}$$

by

$$(x-v)^T M_R^{-1} M_S M_R (x-v) \leq 1 \quad (3)$$

The exact volume is described by $V = \frac{4}{3} \pi abc$. Thus the volume of n disjoint ellipsoids with radii $a_i, b_i, c_i, i \in 1, \dots, n$ can be calculated as

$$V_{total} = \frac{4}{3} \pi \sum_{i=1}^n a_i b_i c_i \quad (4)$$

⁶ <http://depcom.uqac.ca/mhiggins//csdcorrections.html>.

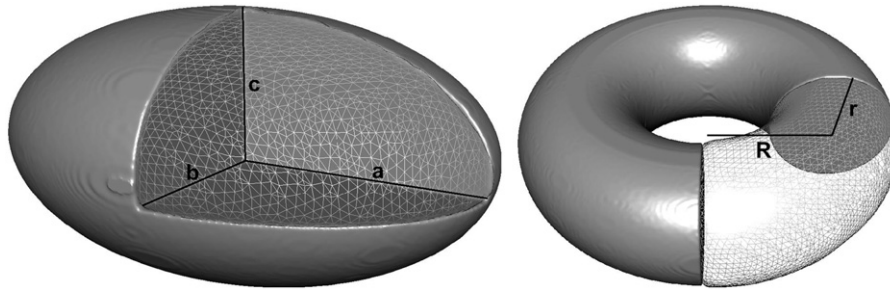


Fig. 9. Ellipsoid and torus parameters.

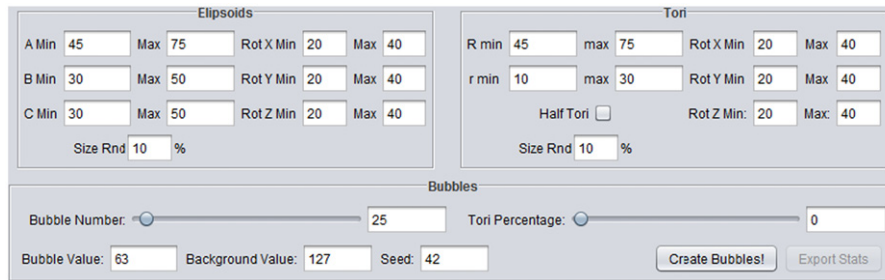


Fig. 10. Virtual volume plugin—user interface.

to minimize the numerical error by factoring out π . Since ellipsoids are convex, the section with a 2D-plane always results in a single connected component.

5.1.2. Half-tori

In the following, a lower index as in v_1, v_2, v_3 describes the component of a vector $v = (v_1, v_2, v_3)^T \in \mathbb{R}^3$. A filled torus, defined by its inner radius r , outer radius R (Fig. 9), centered at v can be described by

$$((x-v)^2 - R^2 - r^2)^2 \leq 4R^2(r^2 - (x-v)_3^2) \quad (5)$$

for $x \in \mathbb{R}^3$. An arbitrarily oriented half-torus can therefore be defined by introducing a rotation matrix $M_R \in \mathbb{R}^{3 \times 3}$. Let $u = (u_1, u_2, u_3)^T = M_R(x-v)$, then

$$(u^2 - R^2 - r^2)^2 \leq 4R^2(r^2 - u_3^2) \quad (6)$$

describes the torus. The same equation describes a half-torus if $u_3 > 0$ is requested.

The volume V_{torus} is calculated by $V_{\text{torus}} = 2\pi^2 R r^2$, thus $V_{\text{half-torus}} = \pi^2 R r^2$. The section of a (half-)torus with a 2D-plane can result in one or two connected components.

5.1.3. Virtual volume plugin

To generate different sufficiently realistic test cases, the virtual volume module was implemented as a plugin for YaDiV. The tool allows to fill a virtual grid with ellipsoid-, tori- and/or half-tori shapes with random or fixed distribution, sizes and orientations (Fig. 10).

The plugin creates torus and ellipsoid shapes defined by the given parameters and avoids shape intersections. Shape parameters and the (exact) volume values can be exported in CSV⁷ format, which can be opened by most database and calculation programs (e.g. Excel or LibreOffice-Calc). Afterwards, the mathematical exact shapes are discretely sampled by a grid of user-defined dimensions,

which can also be exported to a series of slice images similar to a tomographic scan.

5.2. Accuracy analysis: virtual test scan

The virtual test scans used here had resolutions of 1024^3 voxel with grid spacing of 1 mm^3 . The maximum number of objects (referred to as bubbles) was fixed, while the percentage of half-tori varied from zero to 100 in steps of 25%, see Table 1 and Fig. 12. The parameters for ellipsoids and tori, such as radius size, rotation angle and random size, were kept constant. Depending on the angle of intersection for 2D-slice images, half-tori can result in one or two individual areas and directly influence the determined number of objects per unit area, resulting in relatively low or high number densities, respectively. Therefore, half-tori are simplified geometrical shapes to simulate irregular or twinned shapes of objects in natural geological systems. An example is illustrated in Fig. 11(a–c) where a natural hollow crystal is presented as two distinct parallel crystals in the 2D-slice images. However, when segmented and visualized in 3D (Fig. 11(d)), it is clearly seen that there is only one single body.

In Table 1, original, virtual and segmented bubble volume data and BNDs derived from three different evaluation methods are presented. BND values are calculated from the exported csv-files for the produced virtual (original) and for the segmented bubble volume by YaDiV (including volume data of each individual bubble). In addition, the BNDs have been also calculated from the generated 2D-slice images, assuming an ideal ellipsoidal bubble shape or applying the 3D-correction method of Noguchi et al. (2008). The values determined by the three different methods are plotted as a function of the half-tori percentage in Fig. 13.

The total bubble volume segmented with YaDiV and its volume percentage negligibly differ from the original values. BNDs do not show any discrepancy between original and segmented bodies, and are only slightly increasing with increasing half-tori percentage from 2.26 to 2.30 at 0–100%, respectively. BND values derived from 2D-slice image analysis show a

⁷ CSV stands for “comma separated values”, see RFC 4180 Shafraonovich (2005).

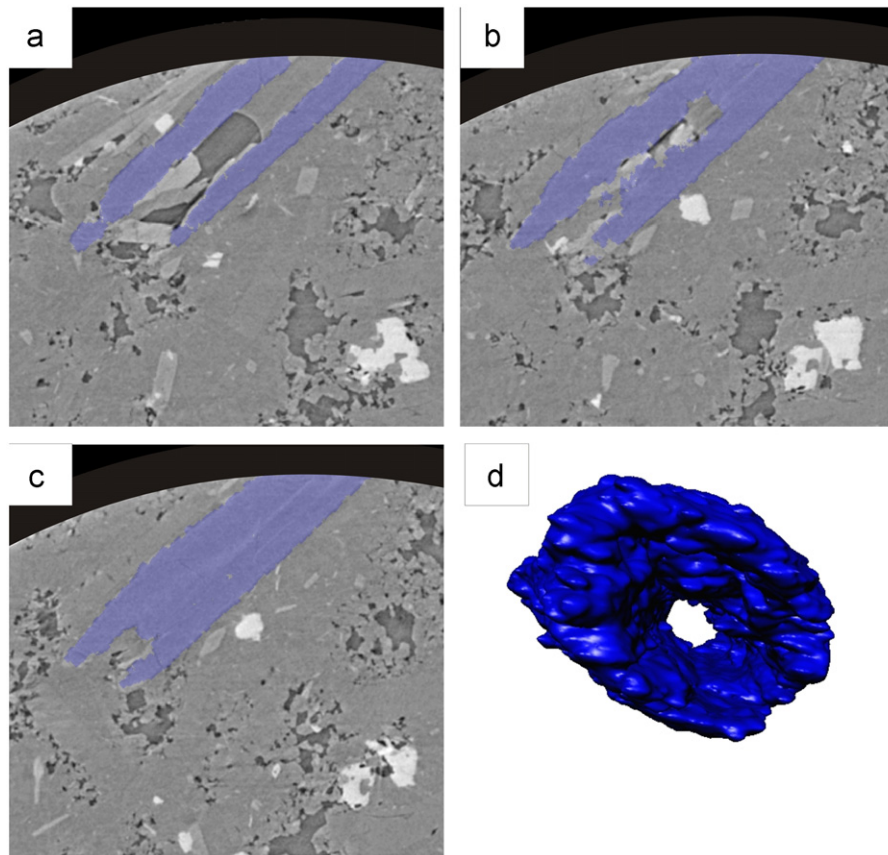


Fig. 11. Example of natural Unzen core samples: (a–c) 2D-slice image of amphibole crystal at different scan depths and (d) 3D-visualization of segmented single hollow amphibole crystal.

Table 1
Parameters and results for virtual samples.

Segment name	Seg-1	Seg-2	Seg-3	Seg-4	Seg-5
<i>Parameters for original virtual test scan</i>					
tori percentage	0	25	50	75	100
Given # ellipsoids	195	138	79	45	0
Given # (half-)tori	0	62	139	174	214
Given total bubble volume (ml)	180,445.389	162,060.0246	136,578.816	121,255.212	97,782.279
Given bubble volume percentage (%)	16.805	15.093	12.720	11.293	9.107
BND value of virtual bubbles (m^{-3})	181.608	186.265	203.028	203.960	199.303
log BND (m^{-3})	2.259	2.270	2.308	2.310	2.300
<i>Segmented parameters (YaDiv)</i>					
Segmented # of single objects (bubbles)	195	200	218	219	214
Segmented total bubble volume (ml)	180,396.022	162,025.444	136,575.047	121,255.281	97,782.226
Segmented volume percentage (%)	16.801	15.090	12.720	11.293	9.107
BND value of segmented bubbles (m^{-3})	181.608	186.265	203.028	203.960	199.303
log BND (m^{-3})	2.259	2.270	2.308	2.310	2.300
Deviation from original log BND (m^{-3})	0.000	0.000	0.000	0.000	0.000
Average area percentage (ImageJ) (%)	18.866	17.043	14.229	12.77	10.083
Standard deviation of replicate analyses	3.460	2.549	1.727	2.050	1.809
<i>Gardner et al. (1999)</i>					
BND (m^{-3})	386.903	440.469	554.383	652.535	838.235
log BND (m^{-3})	2.588	2.644	2.744	2.815	2.923
Standard deviation of replicate analyses	0.068	0.081	0.081	0.101	0.095
Deviation from original log BND (m^{-3})	0.328	0.374	0.436	0.505	0.624
<i>Noguchi et al. (2008)</i>					
BND (m^{-3})	191.760	273.300	570.693	555.749	471.035
log BND (m^{-3})	2.283	2.437	2.756	2.745	2.673
Standard deviation of replicate analyses	0.101	0.127	0.269	0.249	0.194
Deviation from original log BND (m^{-3})	0.024	0.167	0.449	0.435	0.374

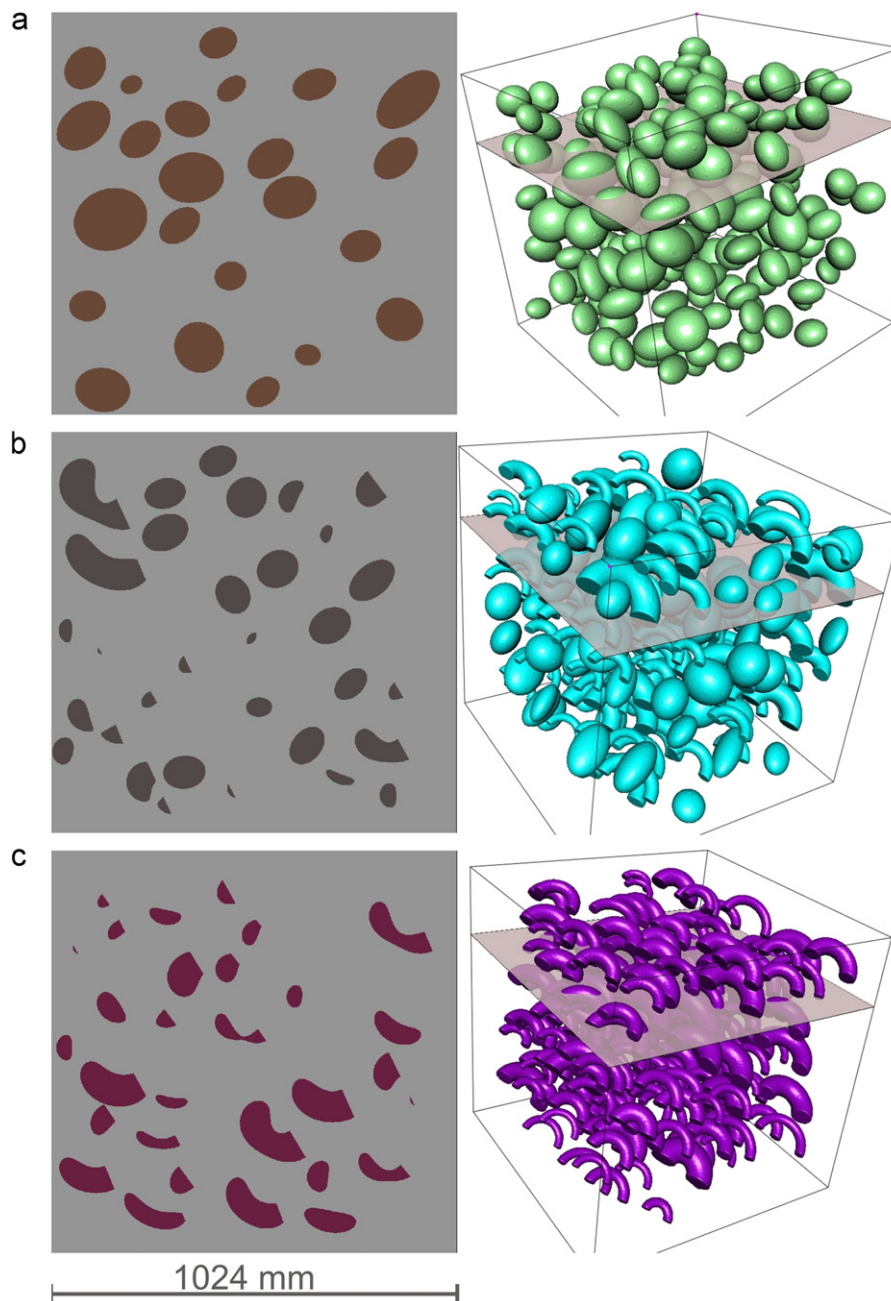


Fig. 12. 2D-images and 3D-visualization of three examples of the virtual test scans: (a) only ellipsoids, (b) ellipsoids and half-tori at 50:50 and (c) only half-tori.

relatively high reproducibility error (± 0.2 – 0.3 log units) after replicate image analysis (9–10 images/scan).

BND data, obtained assuming ideal ellipsoids in all cases, shows a continuous increase with half-tori percentage. The values are about 0.3–0.6 log units higher than the virtually created values and than those determined by 3D-segmentation. The 3D-correction method of [Noguchi et al. \(2008\)](#) results also in large reproducibility errors and in a non-linear trend, see [Fig. 13](#). Such a discrepancy between 2D- and 3D-approaches is a direct illustration of analytical artifacts produced by 2D-to-3D-conversion which can significantly affect the results of the morphological analysis, especially when fundamental parameters (such as aspect ratios and roundness factors) have to be preconditioned and/or generalized for more than one object.

These results are in a good agreement with those of our virtual test scans and with the preliminary assumption that high numbers

of irregular shapes objects (here: half-tori) decrease the accuracy of conventional stereological methods. Hence, we can conclude that at least for the investigated samples the segmentation method implemented in YaDiV is able to produce very accurate and precise textural data.

6. Summary and outlook

We have presented the newly developed YaDiV software that can provide 3D-visualization as well as accurate and precise volume parameter analysis of heterogeneous samples. The software supports fast and interactive visualization methods including support for virtual reality devices, e.g., stereographic visualization providing a natural and intuitive view on volumetric data ([Section 3](#)). It includes segmentation methods to define

certain structures of interest, allowing to analyze volume and shape parameters. We evaluated the quality of these tools in Section 5 and showed that the new 3D-methods lead to a huge exactness improvement over traditional (2D-based) techniques. Finally we demonstrated their usability for practical tasks (Section 4).

First thing that catches the eye when viewing the 3D-segmentation and -visualization of the natural scandata (Section 4)

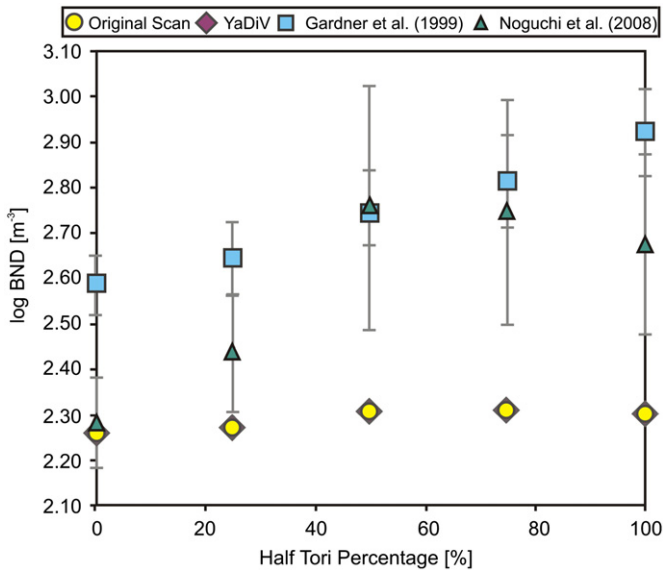


Fig. 13. Comparison of logarithmic bubble number densities (log BND) as a function of the half-tori percentage used for a virtual sample. Error bars show standard deviation (2σ) of replicate 2D-analyses. Errors for 3D-segmentation analyses are negligible.

using YaDiV is the spatial presentation of structures that may not be clear from looking on 2D-images only: especially flow dynamics such as preferred bubble orientation (Fig. 14a–b) or oriented crystallization along a bubble-free crack zone (on the left-hand side in Fig. 14c). But also single shape phenomena, like the hollow crystal in Fig. 14d, can be understood more easily when presented interactively in 3D.

In a next step, we are working on a plugin that identifies the preferred direction of oriented objects within a single segment. In case of Fig. 14a–b, this would concern the orientation of bubbles in our samples, which could give implications on degassing processes (e.g. bubble coalescence or segregation from the melt) relevant to the determination of the eruption style: effusive vs. explosive. We also plan to develop a surface recognition algorithm, i.e., a model-based segmentation method, further simplifying the 3D-segmentation process of geological samples. This algorithm would be especially useful when the quality of tomographic projection images is affected by beam dispersion or by preparation-related cracks, see Fig. 15a and b, respectively.

In conclusion, YaDiV has the following advantages over other available (mostly commercial) 3D-software. (1) The use in the context of science and research is free. (2) It is Open-source and can be enhanced by plugins developed by users with programming skills. The (3) low hardware capacity and (4) unnecessary for installation (runs also from an USB-stick) make YaDiV efficient and portable. (5) Implementation of a variety of image formats. Although quality and quantity of the obtained volume data are dependent on the tomographic technique and on the image resolution also to some degree on the users accuracy, here the listed points 1–5 emphasize the originality of YaDiV as an interactive platform which is designed to be continuously improved by its users, programming their own additional plugins. Thus, YaDiV has the potential to become a universal and popular 3D-instrument in diverse (geological) disciplines, using tomographic data as input.

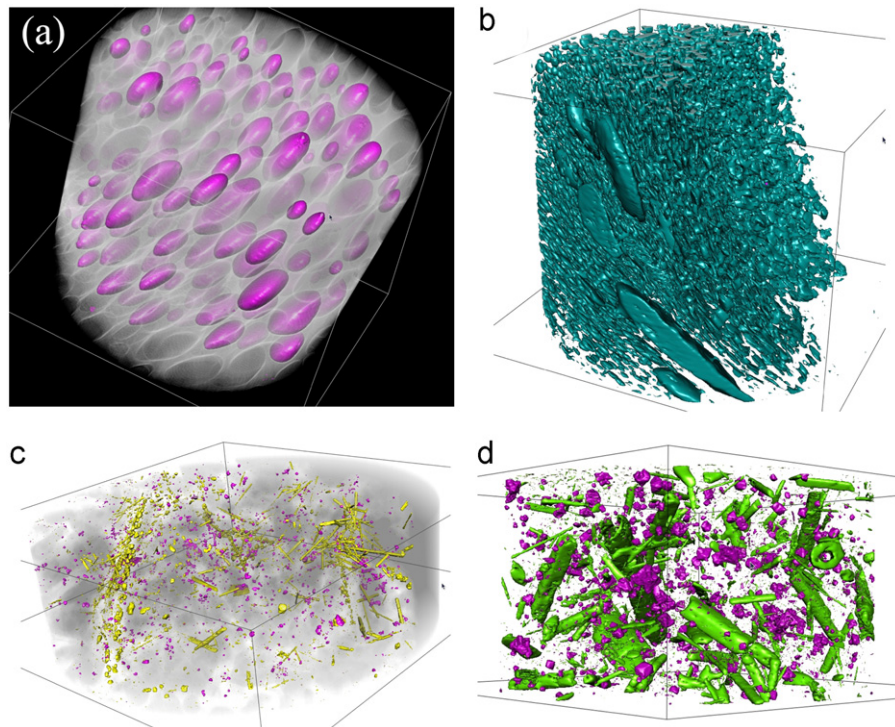


Fig. 14. Screenshots of YaDiV 3D-visualization of different segments. (a) and (b) show spatially oriented elongated bubbles, while (c) visualizes the distribution and orientation of different mineral phases (pyroxenes in yellow, oxides in purple color, gray background represents Texture2d volume rendering of the original data) and in (d) a hollow shape of an amphibole mineral (green) is shown in the upper right corner. Diameter of sample cylinders in (a), (b) and (d) approx. 0.8 mm and diameter in (c) approx. 1.5 mm. (For interpretation of the references to color in this figure caption, the reader is referred to the web version of this article.)

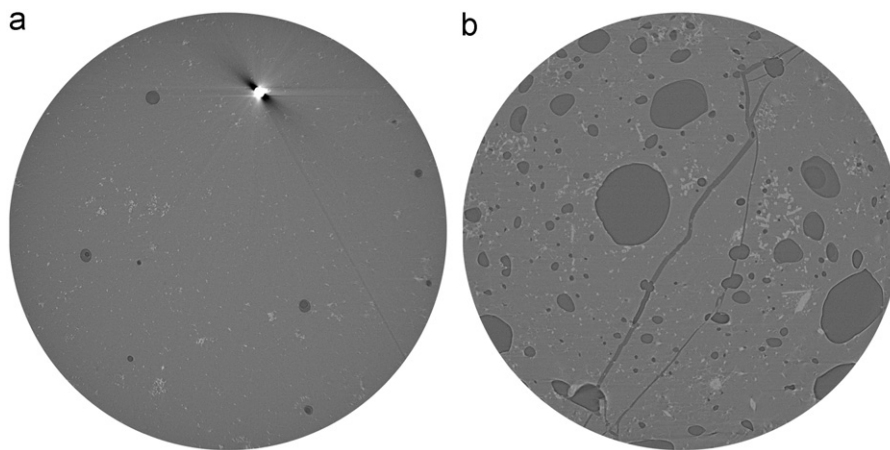


Fig. 15. Tomographic 2D-projection images showing (a) beam dispersion caused by high-density oxide mineral (white color) and (b) cracks caused by the sample preparation.

Acknowledgments

We would like to thank Philipp Blanke, Francois Holtz and Alexander Vais for their support during the work (and time for proofreading). Our appreciation goes to the two anonymous reviewers and the editor D. Vargas for their valuable comments on improving the paper structure. We appreciated very much the technical support from the TOMCAT staff at SLS and thank Stefan Dultz for sharing his beamline time with us, analyzing additional rock samples.

References

- Armentieri, P., 2008. Decryption of igneous rock textures: crystal size distribution tools. *Reviews in Mineralogy and Geochemistry* 69, 623–649.
- Baker, D., Mancini, L., Polacci, M., Higgins, M., Gualda, G., Hill, R., Rivers, M., 2012. An introduction to the application of X-ray microtomography to the three-dimensional study of igneous rocks. *Lithos* 148, 262–276.
- Bruckner, S., Gröller, M.E., 2007. Style transfer functions for illustrative volume rendering. *Computer Graphics Forum* 26, 715–724.
- Carneiro, B.P., Silva, C.T., Kaufman, A.E., 1996. Tetra-cubes: an algorithm to generate 3d isosurfaces based upon tetrahedra. In: *Brazilian Symposium on Computer Graphics and Image Processing, SIBGRAPI 96* 21, pp. 205–210.
- Cichy, S., Botcharnikov, R., Holtz, F., Behrens, H., 2010. Vesiculation and microlite crystallization induced by decompression: a case study of the 1991–1995 Mt Unzen Eruption (Japan). *Journal of Petrology*.
- Cichy, S.B., 2011. Experimental study on vesiculation and formation of ground-mass microlites induced by decompression: constraints on processes related to magma ascent at Unzen volcano. Ph.D. Thesis. Leibniz Universität Hannover, Naturwissenschaftliche Fakultät, Institut für Mineralogie, Germany.
- Cohen, L.D., 1991. On active contour models and balloons. *CVGIP: Image Understanding* 53, 211–218.
- Friese, K.-I., 2010. Entwicklung einer Plattform zur 3D-Visualisierung und -Segmentierung medizinischer Daten. Ph.D. Thesis. Leibniz Universität Hannover, Faculty of Electrical Engineering and Computer Science, Welfenlab, Germany.
- Friese, K.-I., Blanke, P., Wolter, F.-E., 2011. YaDiV—an open platform for 3D visualization and 3D segmentation of medical data. *The Visual Computer* 27, 129–139.
- Gardner, J.E., Hilton, M., Carroll, M.R., 1999. Experimental constraints on degassing of magma: isothermal bubble growth during continuous decompression from high pressure. *Earth and Planetary Science Letters* 168, 201–218.
- Higgins, M.D., 2000. Measurement of crystal size distribution. *American Mineralogist* 85, 1105–1116.
- Higgins, M.D., 2002. Closure in crystal size distributions (CSD), verification of CSD calculations, and the significance of CSD fans. *American Mineralogist* 87, 171–175.
- Higgins, M.D., 2006a. *Quantitative Textural Measurements in Igneous and Metamorphic Petrology*, 1st ed. Cambridge University Press.
- Higgins, M.D., 2006b. Verification of ideal semi-logarithmic, lognormal or fractal crystal size distributions from 2d datasets. *Journal of Volcanology and Geothermal Research* 154, 8–16.
- Kajiya, J.T., Herzen, B.P.V., 1984. Ray tracing volume densities. *SIGGRAPH Computer Graphics* 18, 165–174.
- Kass, M., Witkin, A., Terzopoulos, D., 1988. Snakes: active contour models. *International Journal of Computer Vision* 1, 321–331, <http://dx.doi.org/10.1007/BF00133570>.
- Ketcham, R.A., 2005. Three-dimensional grain fabric measurements using high-resolution x-ray computed tomography. *Journal of Structural Geology* 27, 1217–1228.
- Lorensen, W.E., Cline, H.E., 1987. Marching cubes: a high resolution 3d surface construction algorithm. In: *SIGGRAPH '87: Proceedings of the 14th Annual Conference on Computer Graphics and Interactive Techniques*, ACM Press, New York, NY, USA, pp. 163–169.
- Malladi, R., Sethian, J.A., Vemuri, B.C., 1995. Shape modeling with front propagation: a level set approach. *IEEE Transactions on Pattern Analysis and Machine Intelligence* 17, 158–175.
- McInerney, T., Terzopoulos, D., 1996. Deformable models in medical image analysis: a survey. *Medical Image Analysis*.
- Noguchi, S., Toramaru, A., Nakada, S., 2008. Relation between microlite textures and discharge rate during the 1991–1995 eruptions at Unzen, Japan. *Journal of Volcanology and Geothermal Research* 175, 141–155.
- Nowak, M., Cichy, S., Botcharnikov, R., Walker, N., Hurkuck, W., 2011. A new type of high pressure low-flow metering valve for experiments at continuous decompression: first experimental results for magmatic systems. *American Mineralogist* 96, 1373–1380.
- Polacci, M., Baker, D.R., Mancini, L., Favretto, S., Hill, R., 2009. Vesiculation in magmas from stromboli and implications for normal strombolian activity and paroxysmal explosions in basaltic systems. *Journal of Geophysical Research* 114, <http://dx.doi.org/10.1029/2008JB005672>.
- Rohlfing, T., Brandt, R., Menzel, R., Russakoff, D.B., Maurer Jr., C.R., 2005. Quo vadis, atlas-based segmentation. In: Suri, J., Wilson, D.L., Laxminarayan, S. (Eds.), *The Handbook of Medical Image Analysis—Volume III: Registration Models*. Kluwer Academic/Plenum Publishers, New York, NY, USA, pp. 435–486, Chapter 11.
- Serra, J., 1982. *Image Analysis and Mathematical Morphology*. Academic Press, London, UK.
- Shafraunovich, Y., 2005. Common format and mime type for comma-separated values (CSV) files. RFC 4180 (Informational).
- Sloan, P.P.J., Martin, W., Gooch, A., Gooch, B., 2001. The lit sphere: a model for capturing NPR shading from art. In: Watson, B., Buchanan, J.W. (Eds.), *Graphics Interface 2001*, Canadian Information Processing Society, Toronto, Ont., Canada, Canada, pp. 143–150.
- Smith, A.R., 1995. A pixel is not a little square, a pixel is not a little square, a pixel is not a little square! (and a voxel is not a little cube). Technical Memo TM 6. Microsoft.
- Westover, L., 1991. Splatting: a parallel, feed-forward volume rendering algorithm. Ph.D. Thesis, University of North Carolina at Chapel Hill, USA.